UC Santa Barbara

UC Santa Barbara Previously Published Works

Title

Simulation of the cytoskeletal response of cells on grooved or patterned substrates

Permalink

https://escholarship.org/uc/item/99q0x33p

Journal

Journal of The Royal Society Interface, 12(105)

ISSN

1742-5689

Authors

Vigliotti, A
McMeeking, RM
Deshpande, VS

Publication Date

2015-04-01

DOI

10.1098/rsif.2014.1320

Peer reviewed

eScholarship.org Powered by the California Digital Library
University of California

INTERFACE

rsif.royalsocietypublishing.org

Research

Cite this article: Vigliotti A, McMeeking RM, Deshpande VS. 2015 Simulation of the cytoskeletal response of cells on grooved or patterned substrates. *J. R. Soc. Interface* **12**: 20141320.
http://dx.doi.org/10.1098/rsif.2014.1320

Received: 1 December 2014
Accepted: 19 February 2015

Subject Areas:
biomechanics, biophysics, bioengineering

Keywords:
mechano-sensitivity, cell signalling, focal adhesions, actin/myosin contractility

Author for correspondence:
V. S. Deshpande
e-mail: vsd@eng.cam.ac.uk

Electronic supplementary material is available at http://dx.doi.org/10.1098/rsif.2014.1320 or via http://rsif.royalsocietypublishing.org.

THE ROYAL SOCIETY PUBLISHING

Simulation of the cytoskeletal response of cells on grooved or patterned substrates

A. Vigliotti[1], R. M. McMeeking[2,3] and V. S. Deshpande[1]

[1]Department of Engineering, University of Cambridge, Cambridge CB2 1PZ, UK
[2]Department of Mechanical and Environmental Engineering, University of California, Santa Barbara, CA 93106, USA
[3]School of Engineering, University of Aberdeen, King's College, Aberdeen AB24 3UE, UK

We analyse the response of osteoblasts on grooved substrates via a model that accounts for the cooperative feedback between intracellular signalling, focal adhesion development and stress fibre contractility. The grooved substrate is modelled as a pattern of alternating strips on which the cell can adhere and strips on which adhesion is inhibited. The coupled modelling scheme is shown to capture some key experimental observations including (i) the observation that osteoblasts orient themselves randomly on substrates with groove pitches less than about 150 nm but they align themselves with the direction of the grooves on substrates with larger pitches and (ii) actin fibres bridge over the grooves on substrates with groove pitches less than about 150 nm but form a network of fibres aligned with the ridges, with nearly no fibres across the grooves, for substrates with groove pitches greater than about 300 nm. Using the model, we demonstrate that the degree of bridging of the stress fibres across the grooves, and consequently the cell orientation, is governed by the diffusion of signalling proteins activated at the focal adhesion sites on the ridges. For large groove pitches, the signalling proteins are dephosphorylated before they can reach the regions of the cell above the grooves and hence stress fibres cannot form in those parts of the cell. On the other hand, the stress fibre activation signal diffuses to a reasonably spatially homogeneous level on substrates with small groove pitches and hence stable stress fibres develop across the grooves in these cases. The model thus rationalizes the responsiveness of osteoblasts to the topography of substrates based on the complex feedback involving focal adhesion formation on the ridges, the triggering of signalling pathways by these adhesions and the activation of stress fibre networks by these signals.

1. Introduction

Cells are known to be very sensitive to their mechanical, chemical and topographical environments. For example, mesenchymal stem cells (MSCs) sense and respond to the stiffness of the substrate they are cultured on and differentiate into bone cells when cultured on stiff substrates, but give rise to neuronal cells under identical conditions when soft substrates were used [1]. Similarly, endothelial cells sense stresses and display an increased proliferation rate in regions of high traction [2]. The ability of MSCs to sense their chemical environment was shown by using ligand patterns [3] to limit the spreading of cells. Limiting spreading increases the tendency of MSCs to differentiate into fat cells in contrast to their tendency to become bone cells when allowed to spread. Building on these strategies, McMurray *et al*. [4] embossed substrates to pattern square-shaped pits 120 nm in size, arranged in a square lattice with a separation of 180 nm between the pits. They observed that MSCs cultured on the pitted substrates maintained an undifferentiated state for up to eight weeks, whereas cells on the control (planar) substrates rapidly differentiated into various cell types (mostly bone cells), thus demonstrating that the topography of the substrate too has a profound effect on the preservation of pluripotency.

The cell's cytoskeleton, which influences a broad range of cellular activities in a tension-dependent manner, interacts with the substrate through focal adhesions (FAs)—these multi-protein structures in turn transmit regulatory signals (among

© 2015 The Author(s) Published by the Royal Society. All rights reserved.

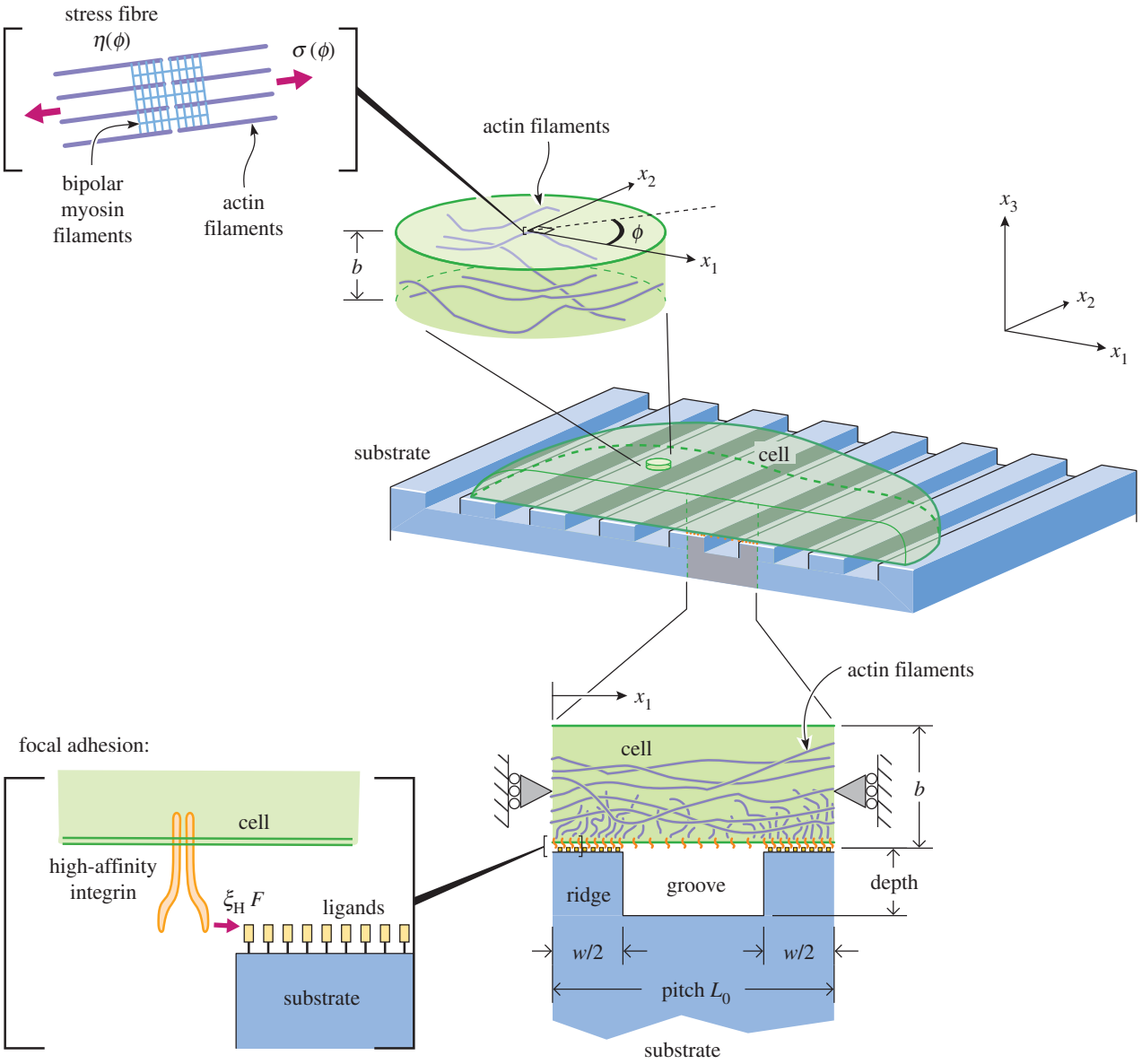

Figure 1. Sketch of the 2D cell on a grooved substrate. The network of stress fibres and the integrin–ligand complexes on the ridges are shown as insets along with the quasi-1D periodic unit cell of the central portion of the cell analysed in this study. The global coordinate system is indicated on the figures with the grooves aligned with the x_2-direction. (Online version in colour.)

them, mechanical signals). For example, a tense cytoskeleton favours differentiation of MSCs into bone cells. The organization and signalling properties of the cytoskeleton can be engineered with nano-patterned substrates: these patterns define the positions, shapes and sizes of the FAs and thereby control the responsiveness of cells to substrate topography. It is thought that similar mechanisms are also employed *in vivo* to control proliferation and differentiation of cells. For example, natural bone ECM (extracellular matrix) is a highly organized nano-composite consisting of, among other things, molecules of type-I collagen. Collagen type-I forms fibrils with an interfibrillar spacing of 68 nm and 35 nm depth [5] and a number of studies [6–8] have demonstrated that mimicking such roughness *in vitro* has beneficial effects on osteoblast proliferation. The role of the collagen fibrillar organization in controlling the arrangement of the actin cytoskeleton has sometimes been referred to as 'contact guidance' [9,10]. In numerous situations [11], contact guidance prevails over mechanical cues such as cyclic stretching in governing the arrangement of the cytoskeleton, confirming the importance of the topographical environment of cells.

The response of cells to substrates with ordered textures has received considerable attention [12–15]. These studies indicate that cells are especially responsive to groove/ridge patterns on the substrate. Of particular note is the study of Lamers *et al.* [16] who created groove patterns (figure 1) that best mimic the *in vivo* length scales of the collagen fibrillar network in natural bone ECM. Their study demonstrated that osteoblasts were responsive to substrates with groove pitches down to approximately 75 nm: at lower pitches the cytoskeletal network was random but with increasing groove pitch the actin filaments of the cytoskeleton increasingly aligned with the groove (or ridge direction). They quantified this observation in terms of the cell orientation with respect to the groove direction on the substrate.

Despite these growing observations of substrate topography governing the cytoskeletal arrangement within cells, no quantitative model to explain these observations, including the so-called phenomenon of contact guidance, has been proposed to-date. Numerous numerical models have been proposed for the remodelling of the cytoskeleton in response to mechanical cues [17–20] and these have successfully predicted the response of cells on a bed of micro-posts [21], subjected to cyclic stretching

[22] and other mechanical loadings such as indentations [23]. Some models have also coupled the stress fibre network with mechano-sensitive FA formation [24] and predicted the FA distributions on substrates with ligand patterns [25]. However, these models all impose an arbitrary spatially uniform activation signal for the cytoskeletal processes. This simplification makes these models unsuitable to predict the response of cells on nano-patterned substrates. Recall that cells sense the topography of their substrates via the feedback between intracellular signalling, cytoskeletal stress fibre formation and FA growth—this combination of mechanisms is critical when models are devised for understanding the development of the cytoskeleton on nano-patterned substrates. Here we use a cooperative feedback model proposed by Pathak *et al.* [26] in order to investigate the development of the stress fibres and FAs for osteoblasts lying on grooved substrates as investigated by Lamers *et al.* [16].

2. Brief description of the bio-chemo-mechanical model

Pathak *et al.* [26] presented a framework for analysing the cooperative feedback loop between signalling, FA formation and cytoskeletal contractility. In the context of a cell placed on a substrate coated with ligands, this loop involves the following four steps:

Step 1. The placement of the cell on a substrate coated with ligands stimulates the formation of FAs on the contact surfaces.
Step 2. The aggregation of proteins within the FA complexes triggers the cascade release of a range of signalling proteins and ions such as Rho, Src and Ca^{2+}.
Step 3. These signalling molecules stimulate cytoskeletal contractility via the formation of actin/myosin stress fibres.
Step 4. The contractile forces generated by stress fibres apply tractions on FAs, which induce further aggregation of integrins in FAs, resulting in additional signalling cascades and consequent cytoskeletal rearrangements.

Here we briefly describe the relevant governing equations and the associated cellular processes in the context of a cell lying on a grooved substrate as in the experiments of Lamers *et al.* [16]. The substrate lies in the x_1-x_2 plane (figure 1) and has grooves along the x_2-direction with a pitch L_0 in the x_1-direction. The ratio between the width w of the ridge and the pitch is denoted by $r \equiv w/L_0$. We envisage a two-dimensional (2D) cell, of thickness b (in x_3-direction) lying on this grooved substrate with adhesive contacts occurring *only along the ridges* (figure 1), i.e. the cell does not sink into the relatively deep grooves, in line with the experiments of Lamers *et al.* [16]. Thus, for the purposes of modelling it suffices to think of a patterned substrate comprising of alternating strips to which the cell can adhere and strips where adhesion is prevented. The dimensions of the cell in the x_1-x_2 plane are assumed to be $\gg L_0$ and here we aim only to model the response of a central portion of the cell far away from the periphery of the 2D cell. Thus, it suffices to model a one-dimensional (1D) unit cell of length L_0 as shown in figure 1 as (i) the response of the central portion of the cell is periodic with period L_0 and (ii) the state of the central portion of the cell is invariant in the x_2-direction with the strain rate $\dot{\varepsilon}_{22} = 0$ in the x_2-direction. The precise boundary conditions will be made explicit subsequently and we now proceed to describe the relevant governing equations in this 1D context.

The interaction of the cell with a substrate incorporates three components that link in a highly nonlinear manner: (i) the activation signal generation, (ii) stress fibre dynamics and (iii) FA dynamics. We shall briefly describe each of these components and readers are referred to the appropriate references quoted in each case for further details of the models.

Signal generation: here we present the 1D version of the signalling model of Pathak *et al.* [26]. We emphasize here that details regarding the precise proteins involved in signalling are not crucial to the mathematical model described below. Rather, the emphasis is on the structure of the reaction–diffusion scheme that provides a positive feedback between FAs and stress fibre formation. Thus, here we reinterpret the Ca^{2+} pathways discussed by Pathak *et al.* [26] in terms of signalling from FAs through Rho GTPase and ROCK (Rho-associated protein kinase) with phosphorylation of NMM2 (non-muscle myosin II).

The main elements of signal activation and transduction phenomena modelled in the cell are: (a) activation of Rho due to the clustering of high-affinity integrins, (b) simultaneous diffusion and dephosphorylation of Rho molecules through the cell, (c) activation of ROCK by the Rho and finally (d) the activation of the intracellular contractile machinery, via ROCK. Processes (a) and (b) are captured via the reaction–diffusion equation (overdot denoting differentiation with respect to time t)

$$\dot{S} = m_s kT \frac{\partial^2 S}{\partial x_1^2} - k_d S + \frac{\alpha}{b} \max(0, \dot{\xi}_H) - S\,\dot{\varepsilon}_{11}, \qquad (2.1)$$

where the first term describes the diffusion of Rho through the cytosol, with S denoting the concentration of Rho in molecules per unit volume, m_s the mobility of Rho molecules in the cytosol, k is Boltzmann's constant and T the absolute temperature. We assume that the dephosphorylation of Rho is described by a first-order reaction with a forward rate constant k_d and a negligible reverse reaction rate. This forward dephosphorylation reaction is modelled by the second term in equation (2.1). The rate of activation of Rho at locations on the cell membrane where high-affinity integrins cluster is described by the third term in equation (2.1). The rate of change of the concentration of high-affinity integrins per unit cell membrane area is denoted by $\dot{\xi}_H$. An increment in ξ_H results in the activation of Rho with a non-dimensional proportionality constant α. Thus, α is interpreted as the number of Rho molecules activated when one low-affinity integrin molecule is converted to its high-affinity configuration.[1] It is worth reminding the readers here that adhesions only occur on the ridges and hence the activation of Rho as described by the third term in equation (2.1) is non-zero only along the ridges of the substrate. The final term describes the change in the concentration of Rho due to the change in the volume of the cytosol under strain. In this 2D setting, the volumetric strain rate reduces to $\dot{\varepsilon}_{11}$, the strain rate in the x_1-direction, as $\dot{\varepsilon}_{22} = 0$ and the third direction is neglected in this analysis.

The Rho diffusing through the cytosol activates ROCK which is also being simultaneously deactivated as it intramolecularly refolds (i.e. process (c) mentioned earlier). We express these kinetics in terms of the normalized activated ROCK concentration $0 \le C \le 1$, where C is the ratio of the activated ROCK concentration to the maximum allowable concentration. Assuming first-order kinetics, the rate of change of C at any location in the cytosol is given as

$$\dot{C} = \lambda_f \frac{S}{S_0}(1 - C) - \lambda_b C, \qquad (2.2)$$

where λ_f is the rate constant governing the unfolding of the ROCK by Rho and S_0 is a reference concentration of Rho. The rate constant λ_b governs the rate at which ROCK is refolded. The kinetic relation (2.2) provides the value of the signal C at any location in the cytosol to initiate cytoskeletal stress fibre rearrangement; i.e. this is the input to a stress fibre contractility model.

Stress fibre contractility model: the bio-chemo-mechanical model of Deshpande *et al.* [17] captures the formation and dissociation of stress fibres, as well as the associated generation of tension and contractility. In this model, actin polymerization (leading to stress fibre formation in the cell) is governed by three coupled phenomena: (i) an activation signal, (ii) tension-dependent stress fibre kinetics and (iii) a force generation mechanism governed by cross-bridge cycling between actin and myosin filaments.

The formation of stress fibres is parametrized by an activation level, designated as η ($0 \le \eta \le 1$) defined as the ratio of the concentration of the polymerized actin and phosphorylated myosin within a stress fibre bundle to the maximum concentrations permitted by biochemistry. The evolution of $\eta(\phi)$ in a direction ϕ with respect to the x_1-axis (figure 1) is characterized by a first-order kinetic equation

$$\begin{aligned}\dot{\eta}(x_1, \phi, t) = k_f C[1 - \eta(x_1, \phi, t)] \\ - k_b\left[1 - \frac{\sigma(x_1, \phi, t)}{\sigma_0(x_1, \phi, t)}\right]\eta(x_1, \phi, t),\end{aligned} \tag{2.3}$$

where k_f and k_b are the forward and backward rate constants, respectively. In this formula, σ is the tension in the stress fibre bundle oriented at angle ϕ while $\sigma_0 \equiv \eta\sigma_{max}$ is the corresponding isometric tension. The stress σ is related to the fibre contraction/extension strain rate $\dot{\varepsilon}(\phi)$ by the cross-bridge cycling between the actin and myosin filaments. A simplified (but adequate) version of the Hill equation [27] is used to model these dynamics and is specified as

$$\frac{\sigma}{\sigma_0} = \begin{cases} 0 & \dfrac{\dot{\varepsilon}}{\dot{\varepsilon}_0} < -\dfrac{\eta}{k_v} \\ 1 + \dfrac{k_v\dot{\varepsilon}}{\eta\dot{\varepsilon}_0} & -\dfrac{\eta}{k_v} \le \dfrac{\dot{\varepsilon}}{\dot{\varepsilon}_0} \le 0 \\ 1 & \dfrac{\dot{\varepsilon}}{\dot{\varepsilon}_0} > 0, \end{cases} \tag{2.4}$$

where the rate sensitivity coefficient, k_v is the fractional reduction in fibre stress upon increasing the shortening rate by $\dot{\varepsilon}_0$. Moreover, the fibre strain rate $\dot{\varepsilon}(\phi)$ is related to the material strain rate via $\dot{\varepsilon} = \dot{\varepsilon}_{11}\cos^2\phi$ as $\dot{\varepsilon}_{22} = \dot{\varepsilon}_{12} = 0$ and the average stress generated by the fibres then follows from a homogenization analysis as

$$\begin{pmatrix} \sigma_{11} & \sigma_{12} \\ \sigma_{12} & \sigma_{22} \end{pmatrix} = \frac{1}{\pi}\int_{-\pi/2}^{\pi/2} \begin{pmatrix} \sigma\cos^2\phi & \dfrac{\sigma}{2}\sin 2\phi \\ \dfrac{\sigma}{2}\sin 2\phi & \sigma\sin^2\phi \end{pmatrix} \mathrm{d}\phi. \tag{2.5}$$

The constitutive description for the stress state within the cell is completed by including contributions from passive elasticity, attributed to intermediate filaments and microtubules of the cytoskeleton attached to the nuclear and plasma membranes. These act in parallel with the active elements, whereupon additive decomposition gives the total stress as

$$\Sigma_{ij} = \sigma_{ij} + \sigma^P_{ij}, \tag{2.6}$$

with the passive stress σ^P_{ij} assumed to be given by a 2D neo-Hookean elasticity model parametrized by the Young's modulus E and Poisson's ratio ν. In terms of the two in-plane principal stretches λ_i the two in-plane principal passive stresses σ^P_i (corresponding to the stress σ^P_{ij}) are given as

$$\sigma^P_i = \frac{E}{4(1+\nu)}J^{-2}(2\lambda_i^2 - I_1) + \frac{E}{2(1-\nu)}(J-1), \tag{2.7}$$

where $I_1 = \lambda_1^2 + \lambda_2^2$ and $J = \lambda_1\lambda_2$. Note that in the unit cell described above, x_1 and x_2 are principal directions and $\lambda_2 = 1$ which greatly simplifies the calculation of σ^P_{ij} from equation (2.7). We note here that for simplicity we only include elastic passive stresses and neglect any viscoelastic effects. This simplification suffices in this study where the focus is on the steady-state response of the cells: at steady-state viscoelastic effects have decayed away and only the elastic passive stresses persist.

Focal adhesion model: Deshpande *et al.* [24] presented a thermodynamically motivated model for the mechano-sensitive formation (and dissociation) of FAs. The model relies on the existence of two conformational states for the integrins: low- and high-affinity states. Only the high-affinity integrins interact with the ligand molecules on the ECM to form complexes. The low-affinity integrins remain unbonded. Since the formation (or dissociation) of the FAs depends on the relative stabilities of the high- and low-affinity integrins, we examine the thermodynamic equilibrium of the two states, which we model as an ideal mixture. The chemical potential of the low-affinity integrins at concentration ξ_L is dependent on their internal energy and configurational entropy in accordance with

$$\chi_L = \mu_L + kT\ln\left(\frac{\xi_L}{\xi_R}\right), \tag{2.8}$$

where μ_L is the reference potential of the low-affinity integrins and ξ_R their reference concentration. For geometrical reasons, the straight architecture of the high-affinity integrins permits the interaction of its receptor with the ligand molecules on the ECM and allows the force transmission between the cell and the substrate. Thus, the high-affinity integrins have an additional contribution to their chemical potential, due to the elastic energy of the integrin–ligand complexes. The ensuing potential is

$$\chi_H = \mu_H + kT\ln\left(\frac{\xi_H}{\xi_R}\right) + \Phi(\Delta) - F\Delta, \tag{2.9}$$

where $\mu_H > \mu_L$ is the reference potential of the high-affinity integrins and $\Phi(\Delta)$ the stretch energy stored in the integrin–ligand complex stretched by Δ via a force $F \equiv \partial\Phi/\partial\Delta$. Spatial gradients in the foregoing chemical potentials motivate the fluxes of the integrins. Two kinetic processes are involved: (i) those governing the rate of conversion of the low-affinity integrins to their high-affinity state (and vice versa) and (ii) diffusive fluxes of the low-affinity integrins along the plasma membrane. The kinetic process (i) is typically fast compared with all other timescales involved and hence we assume local thermodynamic equilibrium between the low- and high-affinity states such that $\chi_H = \chi_L$, while the trafficking of the low affinity is governed by the diffusion equation

$$\dot{\xi} = m\frac{\partial}{\partial x_1}\left(\xi_L\frac{\partial\chi_L}{\partial x_1}\right) - \xi\,\dot{\varepsilon}_{11}, \tag{2.10}$$

where $\xi = \xi_L + \xi_H$ and m is the mobility of the low-affinity integrins along the cell membrane. It now remains to specify the form of the stretch energy $\Phi(\Delta)$ and the relation of Δ to

the displacement u_1 of the 1D cell. Rather than employing a complex interaction, such as the Lennard–Jones potential [28], we use a simple functional form which is a piecewise quadratic potential expressed as

$$\Phi = \begin{cases} \frac{1}{2}\kappa_s\Delta^2 & \Delta < \Delta_n \\ \kappa_s\left(2\Delta_n\Delta - \Delta_n^2 - \frac{1}{2}\Delta^2\right) & \Delta_n \le \Delta \le 2\Delta_n \\ \kappa_s\Delta_n^2 & \Delta > 2\Delta_n, \end{cases} \tag{2.11}$$

where $\gamma \equiv \Phi(\Delta \to \infty) = \kappa_s\Delta_n^2$ is the surface energy of the high-affinity integrins and κ_s the stiffness of the integrin–ligand complex. The maximum force in the integrin–ligand complex, $\kappa_s\Delta_n$ occurs at a stretch $\Delta = \Delta_n$. Finally, the evolution of the stretch Δ is related to the displacement u_1 of the material point on the cell membrane in contact with the ligand patch on the rigid substrate via

$$\dot{\Delta} = \begin{cases} \dot{u}_1 & \Delta < \Delta_n \text{ or } F\dot{\Delta} < 0 \\ 0 & \text{otherwise,} \end{cases} \tag{2.12}$$

where $\dot{\varepsilon}_{11} = \partial\dot{u}_1/\partial x_1$.

Mechanical equilibrium: mechanical equilibrium of the 1D cell stipulates that

$$b\frac{\partial\Sigma_{11}}{\partial x_1} = \xi_H F, \tag{2.13}$$

for the portion of the cell along where adhesions occurs (i.e. along the ridges of the grooved substrate) and F is the force exerted by the cell on the integrin–ligand complex. On the portion of the cell that cannot form adhesions (i.e. the portion of the cell over the grooves), $\partial\sum_{11}/\partial x_1 = 0$. Thus, the total stress Σ_{11} is spatially uniform over the portion of the cell lying over the grooves.

Initial and boundary conditions: we analyse a 1D unit cell of length L_0 as sketched in figure 1 with $x_1 = 0$ corresponding to the left edge. The boundary conditions for the mechanical equilibrium equation (2.13) follow from periodicity as $u_1 = 0$ at $x_1 = 0$ and $x_1 = L_0$. In addition, we assume the state of the central portion of the cell to be invariant in the x_2-direction and thus impose $\varepsilon_{22} = 0$ throughout the cell. Periodicity also dictates that there is no net flow of the activated Rho or the low-affinity integrins out of the unit cell and thus the boundary conditions to equations (2.1) and (2.10) are $\partial S/\partial x_1 = 0$ and $\partial\xi_L/\partial x_1 = 0$, respectively, at $x_1 = 0$ and $x_1 = L_0$.

For simplicity, we assume that the cell is stress, stress fibre and activation signal free at time $t = 0$ which implies that initially $u_1 = \dot{u}_1 = \dot{\varepsilon}_{11} = \eta(\phi) = C = \Sigma_{11} = 0$ throughout the cell. It now remains to specify an initial spatial distribution of the low- and high-affinity integrins. At time $t = 0^-$, the cell is not in contact with the grooved substrate and low- and high-affinity integrins are uniformly distributed over the cell membrane. In this case, the bond stretch $\Delta \to \infty$ such that $F = 0$ and $\Phi = \gamma$. Then, over the entire surface of the cell, equilibrium between the low- and high-affinity integrins specifies

$$\xi_H = \frac{\xi_0}{\exp[(\mu_H - \mu_L + \gamma)/kT] + 1}, \tag{2.14}$$

where $\xi_0 = \xi_L + \xi_H$ is the total integrin concentration at any location on the cell membrane. At time $t = 0^+$, the cell is placed on the grooved substrate which changes the bond stretch to $\Delta = 0$ (and $\Phi = 0$) for the high-affinity integrins in contact with the substrate. Thus, at time $t = 0^+$, the spatial distribution of the integrins is non-uniform and given by equation (2.14) over the domain $w/2 < x_1 < L_0 - w/2$ (i.e. the portion of the cell over the groove where no adhesions form) and by

$$\xi_H = \frac{\xi_0}{\exp[(\mu_H - \mu_L)/kT] + 1}, \tag{2.15}$$

with $\xi_L = \xi_0 - \xi_H$ at locations along the ridges where adhesions form (i.e. over the domains $0 \le x_1 \le w/2$ and $L_0 - w/2 \le x_1 \le L_0$). The increment $\Delta\xi_H$ in the concentration of the high-affinity integrins along the ridges, given by the difference in the values of ξ_H between equations (2.15) and (2.14), will result in Rho activation in the portion of the cell in contact with the substrate. Thus, the initial conditions for S follow as $S = 0$ over $w/2 < x_1 < L_0 - w/2$ and $S = (\alpha/b)\Delta\xi_H$ over the domains $0 \le x_1 \le w/2$ and $L_0 - w/2 \le x_1 \le L_0$. These initial spatial gradients in the integrin concentrations and the initial development of S owing to the action of placing the cell on the substrate will drive the subsequent production of stress fibres, additional FA formation and signalling via the cooperative model detailed above without the need for any artificial external stimuli. The model thus includes both the local and global interactions referred to in Oakes & Gardel [29]: the local forces cause adhesion growth and signalling but these forces are in turn determined by global mechanical equilibrium considerations.

The numerical technique used to solve the above set of coupled partial differential equations is briefly described in the electronic supplementary material.

2.1. Review of the model assumptions

The model makes a number of key assumptions in order to make the problem mathematically and numerically tractable. Here we review some of the key assumptions in view of providing some justifications:

(i) We model the cell using a quasi-1D assumption. This considerably simplifies the solution of the complex coupled equations but also allows for easier interpretation of the results. The 1D assumption which only models the interior of the cell neglects the process of cell spreading that occurs during the early phase of the response of cells on patterned substrates [30]. Moreover, this approach also does not include the differences in adhesions [30] and stress fibres [31] structures between the cell interior and periphery. Thus, the model is restricted to steady-state response of the cell interior.

(ii) We restrict attention to cases where the cell membrane does not dip into and form adhesions within the grooves. Lamers *et al.* [16] show this to be true for grooves with depths $\geq$33 nm. With the effect of the migration of the cell membrane into the grooves neglected, the modelling of the response of cells on grooved substrates reduces to that of cells on patterned substrates where cells only form adhesions on patches that represent the ridges.

3. Material and substrate parameters

All simulations are reported for cells of thickness $b = 1$ μm at a temperature $T = 310$ K with the period L_0 of the grooves varied as a parameter over the range 0.05 μm $\le L_0 \le$ 2.0 μm. Unless otherwise specified we keep the ratio $r \equiv w/L_0 = 0.5$ as in the experiments of Lamers *et al.* [16] and assume the substrates to be rigid. Parameters for the signalling model are inferred from [32] to be the reference Rho concentration

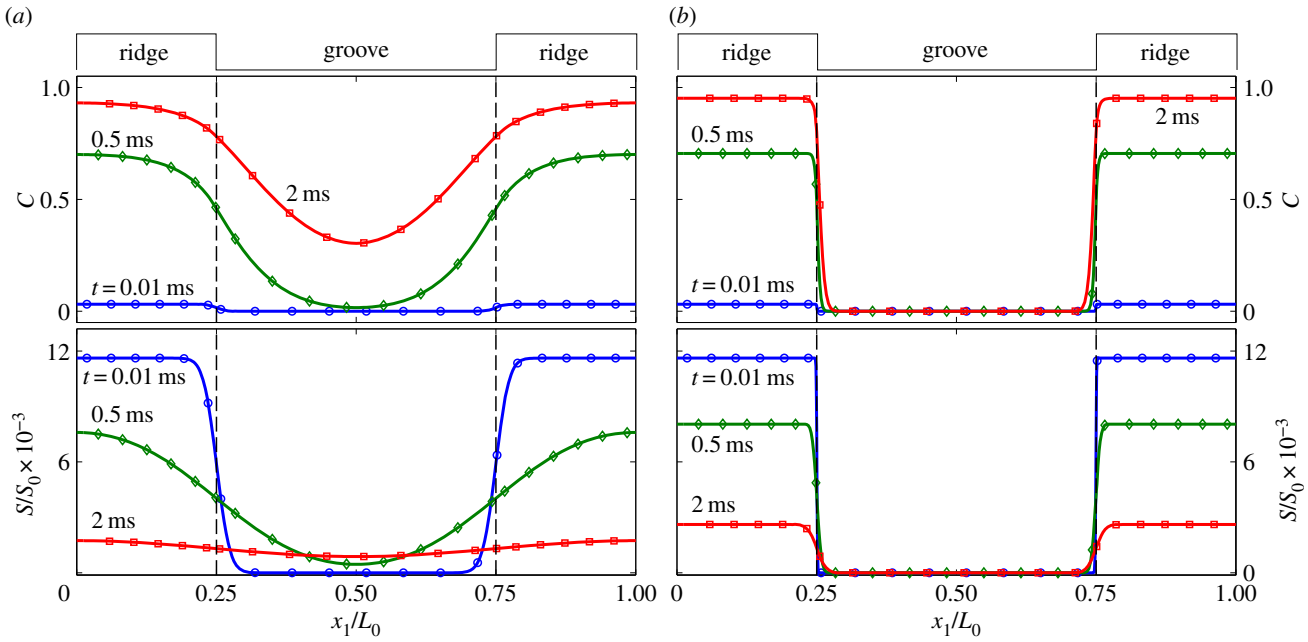

Figure 2. The spatial distributions of the signal levels S/S_0 and C at three selected times $t \leq 2$ ms for the cells on substrates with pitches (*a*) $L_0 = 0.05$ μm and (*b*) $L_0 = 1$ μm. Time $t = 0$ corresponds to the instant the cell was placed on the substrate. (Online version in colour.)

$S_0 = 1000$ molecules μm^{-3} (i.e. approx. 2 μM) with the proportionality constant $\alpha = 1.75$. The mobility of Rho is extremely high with $m_s = 10^4$ s mg^{-1}. Moreover, the unfolding of ROCK by Rho is very rapid but the refolding of ROCK is relatively slow and thus we assume $\lambda_f \gg \lambda_b$, with $\lambda_f = 2.5 \times 10^5$ s^{-1} and $\lambda_b = 0.015$ s^{-1}. The reference value of the rate constant governing the dephosphorylation of Rho is taken as $k_d = 750$ s^{-1} but we report simulations where this parameter is varied to investigate the sensitivity of the results to k_d. The parameters for the FA model are obtained from [33–36]. The resting integrin concentration is $\xi_0 = 1000$ integrins μm^{-2} and the difference in the reference potentials between the high- and low-affinity integrins is taken to be $\mu_H - \mu_L = 5kT$. The mobility of the low-affinity integrins is significantly less than Rho with $m = 10$ s mg^{-1} while the stiffness of the high-affinity/ligand bonds is $\kappa_s = 15$ pN μm^{-1} with a peak force $\kappa_s \Delta_n = 1.95$ pN. The parameters for the cellular contractility model are taken based on the calibrations performed by McGarry *et al.* [21] for osteoblasts with a passive elastic modulus $E = 4$ kPa and $\nu = 0.45$ The maximum stress fibre stress is $\sigma_{max} = 2.5$ kPa while the Hill model parameters are $k_v = 3$ and $\dot{\varepsilon}_0 = 2.8 \times 10^{-4}$ s^{-1}. The rate constants for the stress fibre kinetics are $k_f = 0.03$ s^{-1} and $k_b = 0.1k_f$.

4. Simulations of cell response on grooved substrates

The action of placing the cell on the grooved substrate initiates the signalling process that prompts the cascade of contractility, FA formation and further signalling as described above. The model parameters listed in §3 result in processes occurring over three timescales: (i) the diffusion of Rho that occurs on the order of a few milliseconds; (ii) the unfolding of ROCK that occurs on the same timescale as the Rho diffusion, but its refolding and consequent deactivation occurs on the order of a few minutes and (iii) the stress fibre kinetics that occur on the order of hours. While we do not model the cell periphery where the short-timescale processes dominate we emphasize here that these fast Rho diffusion and ROCK activation processes are the key triggers for the slower stress fibre kinetic processes in the interior of the cell modelled here. We now proceed to discuss these processes for the two extreme values of $L_0 = 0.05$ μm and 1 μm so as to first explain two extreme types of responses.

First consider the early time response on the order of a few milliseconds. In this timescale there is no significant evolution of the FAs or stress fibres while the activated Rho and unfolded ROCK concentrations have responded to the action of the placement of the cell on the grooved substrate. The spatial distributions of S/S_0 and C are included in figure 2*a*,*b* for the $L_0 = 0.05$ μm and 1 μm cases, respectively. In each case predictions are shown for three selected values of time t, where $t = 0$ corresponds to the instant the cell was placed on the substrate. First consider the $L_0 = 0.05$ μm case. At time $t = 0^+$, the initial condition described above implies that $S = \alpha \Delta \xi_H / b$ over the domains $0 \leq x_1/L_0 \leq 0.25$ and $0.75 \leq x_1/L_0 \leq 1$ and $S = 0$ over the central section where the cell covers the groove. Subsequently, the Rho begins to rapidly diffuse towards the central section while it is simultaneously being dephosphorylated at the rate $k_d S$. This is clearly seen in figure 2*a* where the concentration S is reducing across the portion of the cell over the ridges but increasing over the portion of the cell above the grooves. However, for $t > 2.0$ ms, the dephosphorylation rate even in this central section becomes higher than the influx rate of the Rho and the concentration S decreases throughout the cell and reduces to zero everywhere for $t \geq 3.5$ ms. We note that at these early times there is nearly no response from the stress fibres, hence no new FAs form and thus there is no further Rho activation. Now consider the corresponding evolution of the unfolded ROCK concentration. At time $t = 0$, $C = 0 \; \forall x_1$ and then begins to rise in response to the local Rho concentration. The kinetics of ROCK is slower and hence the ROCK concentration continues to increase even as the Rho concentration decreases and begins to

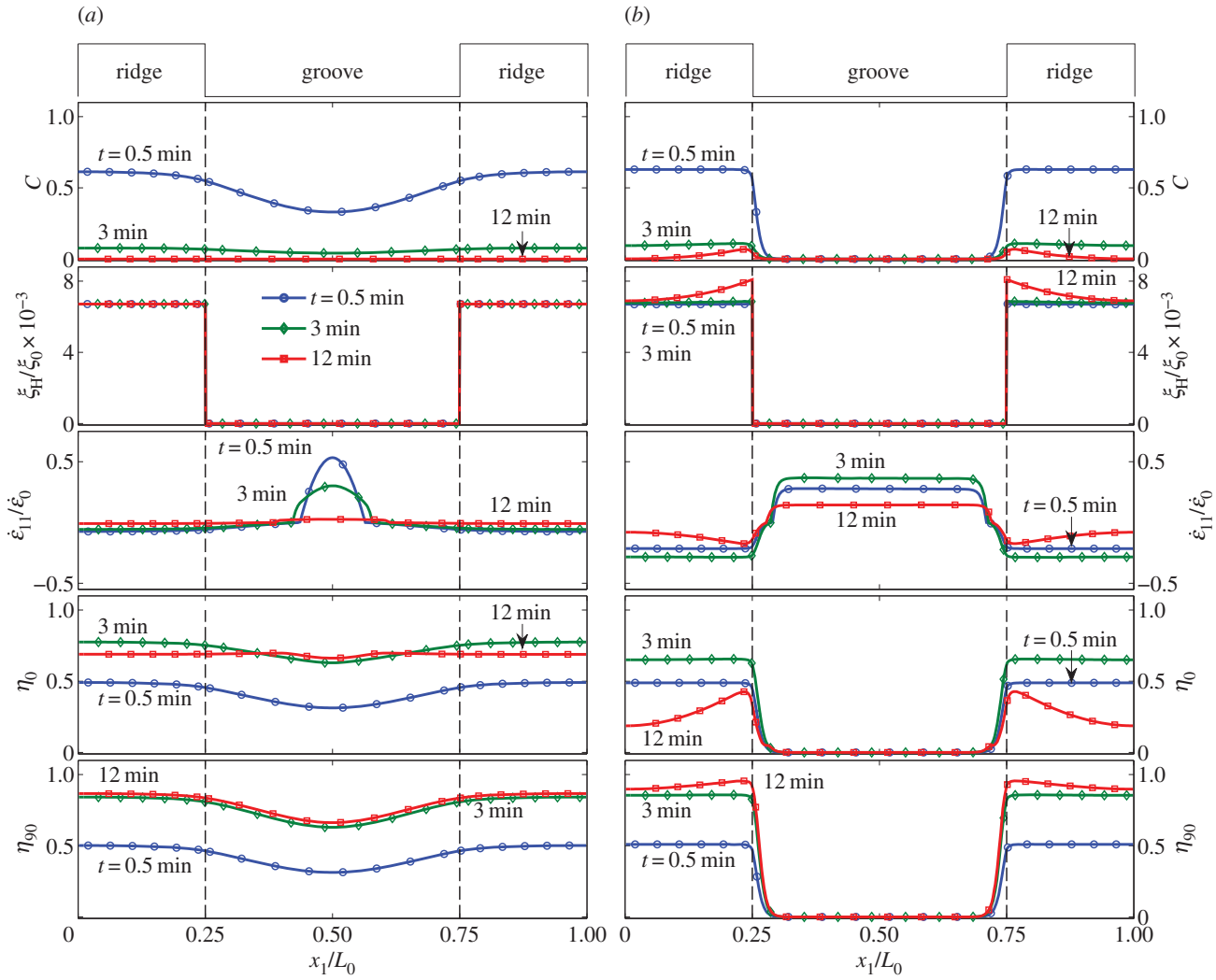

Figure 3. The spatial distributions of C, ξ_H/ξ_0, $\dot{\varepsilon}_{11}/\dot{\varepsilon}_0$ as well as the stress fibre concentrations η_0 and η_{90} for three selected values of the time $t \leq 12$ min for cells on substrates with pitches (*a*) $L_0 = 0.05$ μm and (*b*) $L_0 = 1$ μm. Time $t = 0$ corresponds to the instant the cell was placed on the substrate. (Online version in colour.)

become more spatially uniform. Over the timescale of figure 2*a*, the process of refolding of ROCK has no significant effect and hence C has not begun to decrease. The evolution of S and C for the $L_0 = 1$ μm case is similar with one major difference. The large length implies that the Rho is dephosphorylated prior to it reaching the central portion of the cell over the groove. Thus, both S and C are approximately zero over the section $0.25 < x_1/L_0 < 0.75$ (expect for a small boundary layer near the edges of the ridges).

Now consider the response over the time frame of minutes when $S \approx 0$ owing to it having been largely dephosphorylated. In figure 3, we plot predictions of the spatial distributions of C, the FAs as parametrized by ξ_H/ξ_0 , the strain rate $\dot{\varepsilon}_{11}/\dot{\varepsilon}_0$ and the stress fibre concentrations η_0 and η_{90} in the $\phi = 0^\circ$ and $\phi = 90^\circ$, respectively, for three selected values of the time t. First consider the $L_0 = 0.05$ μm case in figure 3*a*. The ROCK concentration C is spatially relatively homogeneous and decreases throughout the cell over the timescales shown here. On the other hand, the FAs, as parametrized by the normalized concentration ξ_H/ξ_0, are spatially uniform over the ridges (and approximately zero over the grooves where no adhesions form) and do not change on the timescale of the plots in figure 3*a*. This is consistent with the observation that $\dot{\varepsilon}_{11} \approx 0$ over the ridges which implies that there is no additional stretching of the integrin–ligand bonds over these timescales and, therefore, the FAs are reasonably static. However, tensile strain rates are present in the central portion of the cell over the grooves for $t \leq 3$ min, balanced by small contractile strain rates over the remainder of the cell as the total length of the portion analysed does not change. The stress fibre distributions are reasonably isotropic with $\eta_0 \approx \eta_{90}$ throughout the cell though the stress fibre concentrations are slightly lower in the central portion due to the lower levels of signal C in this part of the cell.

Now consider the $L_0 = 1$ μm case in figure 3*b*. Recall that the Rho does not diffuse into the central portion of this cell over the groove. Thus, the ROCK concentration C, as well as the stress fibre concentrations, η_0 and η_{90}, vanish over this central section. The absence of stress fibres results in tensile strain rates over the central section and corresponding contractile rates $\dot{\varepsilon}_{11}$ over the ridges where stress fibres form and contract. These strain rates result in stretching of the integrin–ligand bonds especially near the edges of the ridges at the larger values of t (e.g. $t = 12$ min in figure 3*b*), producing both an increment in the FA concentration at those locations and a corresponding rise in the ROCK concentration C. Consider now the stress fibre kinetics. Stress fibres in this case only form on the ridges where there exists a non-zero signal. Early in the deformation history (i.e. $t = 0.5$ min) the stress fibre distributions on the ridges are nearly isotropic with $\eta_0 \approx \eta_{90}$.

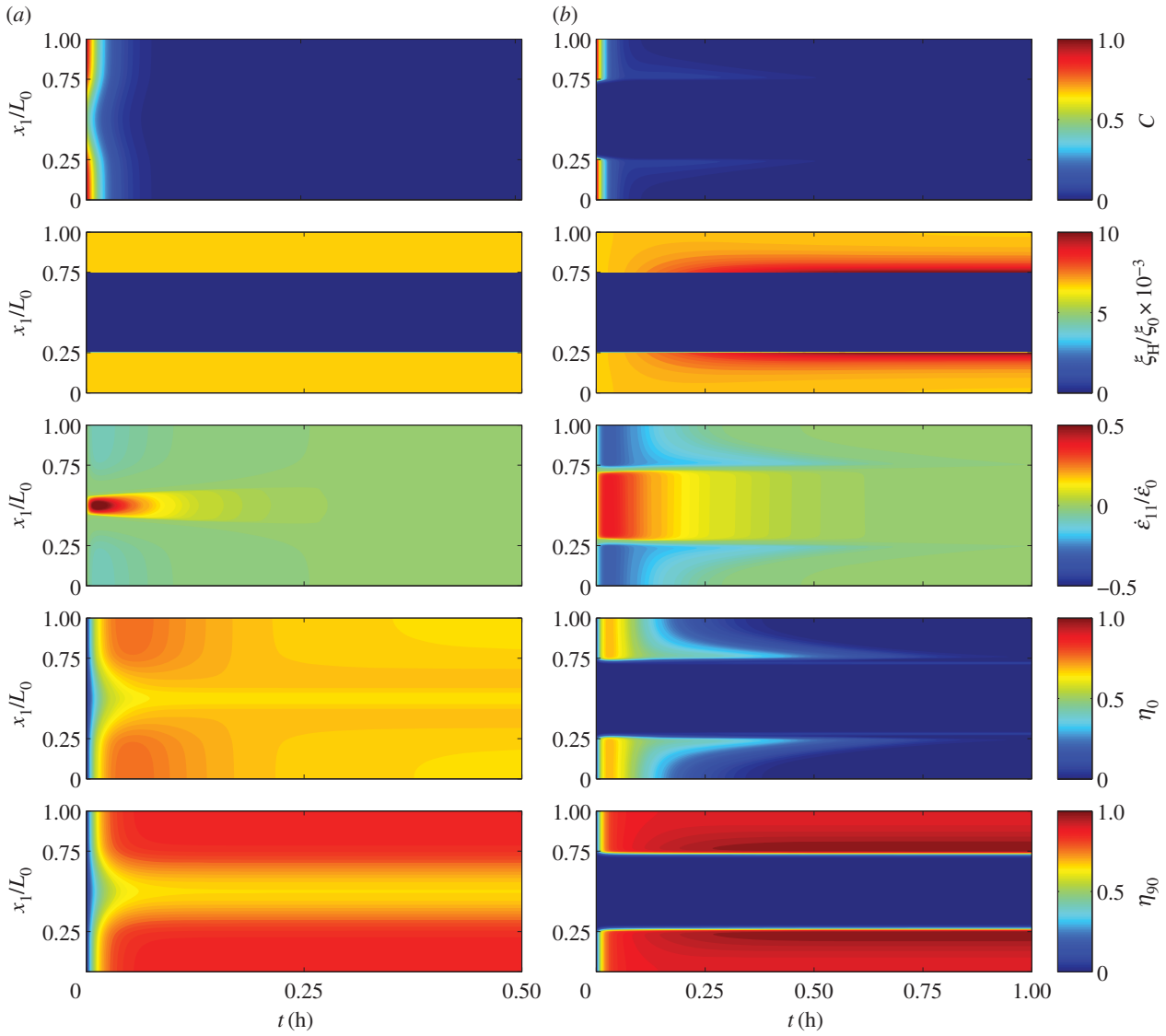

Figure 4. Contour plots of the spatio-temporal distributions of C, ξ_H/ξ_0, $\dot{\varepsilon}_{11}/\dot{\varepsilon}_0$ as well as η_0 and η_{90} for cells on substrates with pitches (*a*) $L_0 = 0.05$ µm and (*b*) $L_0 = 1$ µm during transient. Time $t = 0$ corresponds to the instant the cell was placed on the substrate. Recall that the groove spans the range $0.25 \leq x_1/L_0 \leq 0.75$.

However, as time proceeds the fibres in the $\phi = 0^\circ$ direction dissociate due to the contractile strain rates $\dot{\varepsilon}_{11}$ (and relatively low values of C) but the fibres in the $\phi = 90^\circ$ direction continue to form due to a low persistent signal C and aided by the fact that the dissociation rate in this direction is zero as $\dot{\varepsilon}_{22} = 0$.

A more detailed and comprehensive history of the evolution of C, ξ_H/ξ_0, $\dot{\varepsilon}_{11}/\dot{\varepsilon}_0$ as well as η_0 and η_{90} are shown in figure 4*a*,*b*, respectively, for the $L_0 = 0.05$ µm and 1 µm cases. Contours of the distributions of these quantities are shown in figure 4 where the horizontal axes indicates the time (now in units of hours), while on the vertical axes we plot the normalized position x_1/L_0. For the $L_0 = 0.05$ µm case, it is clear that the signal C has decayed early in the time history ($t \leq 0.05$ h) and the FAs too have attained their final distribution very early. However, the stress fibre concentration η_{90} attains its steady value over a time of about 0.12 h owing to the slower kinetics of the stress fibre formation. The relaxation rates implicit within the Hill relation are even slower, which implies that the strain rate $\dot{\varepsilon}_{11}$ drops to zero over a timescale of about 0.5 h and thus this is also the timescale over which η_0 attains its steady-state value. Qualitatively this time history is similar to the $L_0 = 1$ µm case (figure 4*b*), with two major caveats: (i) the presence of the unfolded ROCK is clearly restricted to the ridges, and the additional stretching of the integrin–ligand bonds due to the longer groove spacing results in additional signal generation[2] and (ii) this additional signalling takes place on the timescale of stress fibre contraction, which delays the attainment of steady state in the $L_0 = 1$ µm case to nearly 1 h. In this context recall that the analysis reported here only models the central portion and not the periphery of the cell. Thus, consistent with observations the model predicts that nearly no adhesions form in the central portion of cell for substrates with $L_0 = 0.05$ µm other than those formed at time $t = 0^+$ by the action of placing the cell on the substrate (the cell periphery where adhesions are observed in such cases is not modelled here). On the other hand, adhesions form over a timescale of approximately 0.5 h in the central portion of cells on the $L_0 = 1$ µm substrates. This slow adhesion growth is consistent with observations [30] for cells on patterned substrates.

The steady-state spatial distributions of stress fibre concentrations, η_0 and η_{90}, are included in figure 5*a*,*b* for the $L_0 = 0.05$ µm and 1 µm cases, respectively. Also included in figure 5 are insets showing circular histograms (similar to

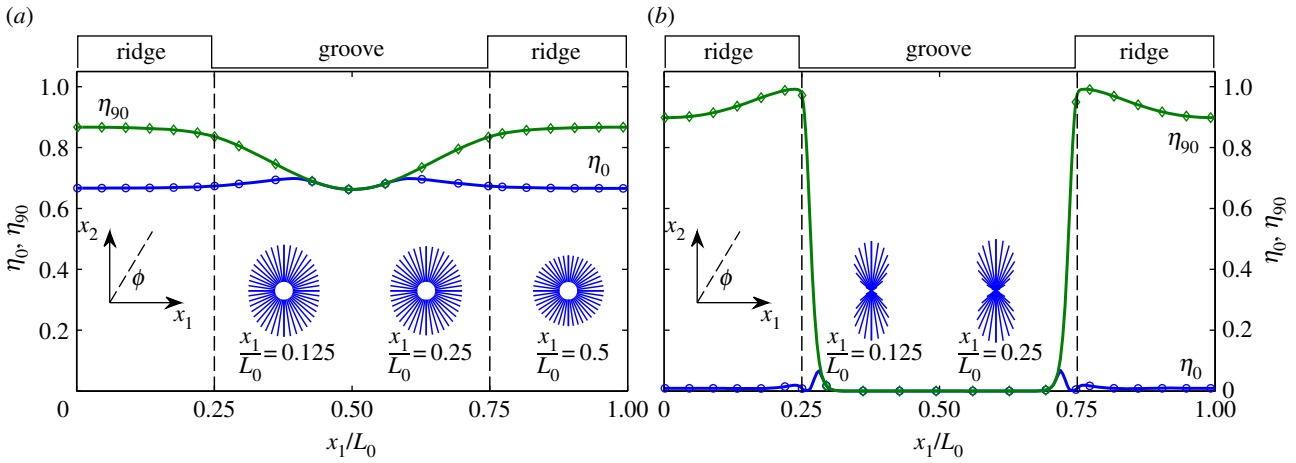

Figure 5. The spatial distributions of the stress fibre concentrations η_0 and η_{90} at steady state for cells on substrates with pitches (*a*) $L_0 = 0.05$ µm and (*b*) $L_0 = 1$ µm. Circular histograms of η at steady state are included as insets at three selected locations within the cell. The histogram at $x_1/L_0 = 0.5$ is omitted in (*b*) as $\eta \approx 0\ \forall\ \phi$ in this case. (Online version in colour.)

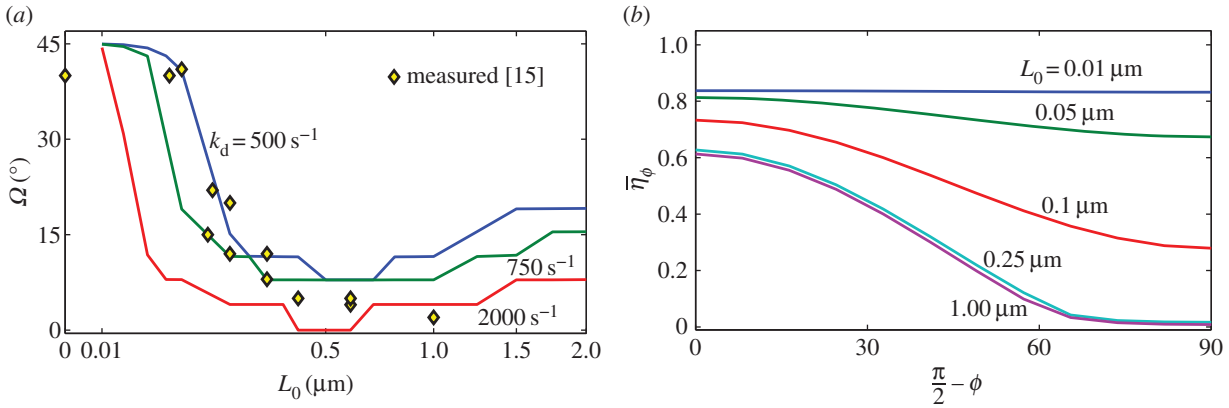

Figure 6. (*a*) Comparison between the measured [16] and predicted values of the cell orientation Ω as a function of the pitch L_0 ($r = 0.5$) for four choices of the dephosphorylation rate constant k_d. (*b*) Predictions of $\bar{\eta}_\phi$ as function of $\pi/2 - \phi$ for selected values of L_0 ($r = 0.5$) and the reference value of k_d. (Online version in colour.)

those introduced in [22,37]) of η at three locations along the cell: $x_1/L_0 = 0.125$ (mid-point of the ridge); $x_1/L_0 = 0.25$ (edge of the ridge) and $x_1/L_0 = 0.5$ (mid-point of the groove). These histograms visually quantify the degree of anisotropy in the distribution of the stress fibres. Clearly for the $L_0 = 0.05$ µm case the steady-state distribution of the stress fibres is both nearly isotropic and spatially uniform. This implies that stress fibres form not only along the ridges but also bridge across the grooves from ridge-to-ridge as seen in figure 4*c* of Lamers *et al.* [16]. By contrast, the steady-state distribution of the stress fibres in the $L_0 = 1$ µm case is both anisotropic and spatially inhomogeneous with fibres only forming on the ridges. On these ridges, the angular distribution of fibres shows a higher concentration in the $\phi = 90°$ direction and almost no stress fibres forming in the $\phi = 0°$ direction. This lower concentration of η_0 is due to the fact that the Rho is dephosphorylated before it can reach the central portion of the cell over the groove, which prevents the formation of a stable stress fibre bundle across grooves as in the $L_0 = 0.05$ µm case. This implies that stress fibres forming over the ridges at $\phi = 0°$ are free to contract as there are no stress fibres in the cell over the groove to balance their contractile forces. This contraction results in the dissociation of the stress fibres in the $\phi = 0°$ direction, and consequently, lower concentrations of η_0 remain above the ridges at steady state. It is worth emphasizing here that unlike in the $L_0 = 0.05$ µm case, stress fibres do not bridge over the grooves in the $L_0 = 1$ µm case. Thus, long continuous stress fibres will primarily be observed only around the $\phi = 90°$ direction over the ridges for cells on the $L_0 = 1$ µm substrates.

Animations showing the evolution of the C, ξ_H/ξ_0, $\dot{\epsilon}_{11}/\dot{\epsilon}_0$, η_0 and η_{90}, as well as the circular the distribution of η at selected locations within the cells are included in the electronic supplementary material.

4.1. Predictions of cell alignment and comparisons with measurements

One of the key findings of the experiments of Lamers *et al.* [16] was the change in the cell orientation as a function of the groove width L_0. In order to quantify cell orientation Lamers *et al.* [16] fluorescently stained the actin filaments and then measured the orientation of the dominant filaments with respect to the ridge direction. We denote this orientation as Ω and replot the measured median values of Ω as a function of L_0 in figure 6*a*. In figure 6*a*, a

nonlinear x-axis scale, $\sqrt{L_0}$, has been employed in order to improve the visualization of the data. A median value of $\Omega = 45^\circ$ indicates a random orientation while $\Omega = 0^\circ$ indicates that the cells are primarily aligned with the ridge (or groove) directions. The measurements clearly show that while cell orientation is random for $L_0 \leq 0.1\ \mu$m, there is a sharp transition at $L_0 \approx 0.1\ \mu$m with the cells being primarily aligned with the ridge direction at higher values of L_0.

The model predictions discussed above clearly indicate that cells form nearly isotropic stress fibre distributions at small values of L_0, but form anisotropic distributions with high stress fibre concentrations in the $\phi = 90^\circ$ direction (i.e. aligned with the ridge direction) for large values of L_0. This indicates that the model is predicting cell orientations that are at least qualitatively consistent with the observations of Lamers *et al.* [16]. In order to make more quantitative comparisons we attempt to interpret the predictions of the model in a manner analogous to the observations reported by Lamers *et al.* [16]. We first define an average stress fibre concentration in any particular direction as

$$\bar{\eta}_\phi \equiv \frac{1}{L_0}\int_0^{L_0} \eta(\phi)\mathrm{d}x_1. \tag{4.1}$$

Predictions of $\bar{\eta}_\phi$ as a function of $\pi/2 - \phi$ are plotted in figure 6*b* for selected values of L_0 (we choose the abscissa of $\pi/2 - \phi$ rather than ϕ so as to be consistent with the definition of cell orientation Ω employed by Lamers *et al.* [16]). It is clear that for small values of L_0, $\bar{\eta}_\phi$ is reasonably independent of ϕ but at larger values of L_0, $\bar{\eta}_\phi$ decreases sharply with increasing $\pi/2 - \phi$. Moreover, the $\bar{\eta}_\phi$ distributions are reasonably insensitive to the value of L_0 for $L_0 > 0.25\ \mu$m. Thus, consistent with the experimental observations, the predictions in figure 6*b* suggest that the cell has stress fibres over the entire range of orientations, but some orientations are dominant with higher values of $\bar{\eta}_\phi$. It thus remains to quantity these dominant orientations in a manner as analogous as possible to the procedure employed by Lamers *et al.* [16].

In cell observations using epifluorescence or confocal microscopes, the fine meshwork of actin is expected to not be visible, i.e. if $\bar{\eta}_\phi$ is less than a critical value, fibres in that orientation are likely to be missed in most observations. We define this critical value of $\bar{\eta}_\phi$ above which fibres are visible to be 50% of the maximum value, i.e. only fibres with $\bar{\eta}_\phi \geq 0.5$ will be visible. We now define a new observable stress fibre distribution as

$$\Gamma_\phi \equiv \begin{cases} \bar{\eta}_\phi & \bar{\eta}_\phi \geq 0.5 \\ 0 & \text{otherwise.} \end{cases} \tag{4.2}$$

Then, similar to Lamers *et al.* [16], the cell orientation Ω is defined as the mean value

$$\Omega = \frac{\pi}{2} - \frac{\int_0^{\pi/2} \phi\Gamma_\phi \mathrm{d}\phi}{\int_0^{\pi/2} \Gamma_\phi \mathrm{d}\phi}. \tag{4.3}$$

The predicted values of cell orientation using this definition of Ω are included in figure 6*a* for three selected values of the dephosphorylation rate constant k_d, including the reference value of $k_\mathrm{d} = 750\ \mathrm{s}^{-1}$. It is clear that the predictions are in reasonable agreement with the measurements for k_d values in the range $500\ \mathrm{s}^{-1} \leq k_\mathrm{d} \leq 750\ \mathrm{s}^{-1}$. Recall that there are some uncertainties in the model parameters and in the metrics used to compare the predictions and observations. Given these uncertainties, the key conclusion of the model is that the lower limit of the groove spacing for an interaction between the grooves and the cells is $L_0 \approx 0.1\ \mu$m but the interaction is definitely lost with cells orienting randomly on substrates for groove spacings $L_0 < 50$ nm.

The predictions in figure 6*a* extend to values of L_0 higher than those investigated by Lamers *et al.* [16]. These predictions seem to indicate that at $L_0 > 1\ \mu$m, the cells will slowly begin to reorient themselves away from the ridge directions. We demonstrate in the electronic supplementary material that this reorientation is due to additional signal production that occurs because of the enhanced contractility (resulting in increased stretching of the integrin–ligand bonds) of the cells at large values of L_0.

The predictions discussed above demonstrate the fidelity of the model in estimating the response of cells on grooved substrates. The key ingredient that enables the model to capture this behaviour is that it includes a spatially inhomogeneous activation signal that arises from the fact that Rho activation only occurs at the FA sites, i.e. only along the ridges in the case of a grooved substrate. The consequences of this are that (i) reducing the ratio r of the width of the ridge to the groove results in a higher level of alignment of the cells with the grooves as there is insufficient signal production to allow for fibres that bridge across the grooves to form and (ii) models that use spatially uniform signals for the activation of stress fibres (e.g. [17–20]) would not only predict that the stress fibre network is spatially uniform for cells on a grooved substrate but also that the network is isotropically distributed for all values of L_0, i.e. $\Omega = 45^\circ\ \forall L_0$. These aspects of the model are further elucidated in the electronic supplementary material.

5. Concluding remarks

The response of osteoblasts on grooved substrates is investigated via a model that accounts for the complex feedback between FA formation on the ridges, the triggering of signalling pathways by the formation of these adhesions and the development of the stress fibre network due to these activation signals. The distance over which signalling proteins activated at the adhesions on the ridges diffuse into the remainder of the cytosol (prior to being dephosphorylated) governs the formation of the actin network. For small groove pitches (less than approx. 100 nm), the signalling proteins diffuse throughout the cytosol resulting in a reasonably spatially homogeneous and isotropic stress fibre network. Thus, the orientation of cells in such cases is random. By contrast, when the groove pitch is large (on the order of 1 μm) the signalling proteins dephosphorylate before they can diffuse into the portion of the cell over the grooves. Therefore, in this case not only does the cytoskeletal network form mainly on the ridges but also the fibres are mainly aligned with the direction of the ridges (or grooves). This results in the cells orienting themselves so as to be aligned with the grooves. The model thus provides a possible explanation for the observations of Lamers *et al.* [16] on the basis of the spatial inhomogeneity of the activation signal for stress fibres. In particular, it shows that the lower limit of the groove spacing for an interaction between the grooves and the cells is about 100 nm but the interaction is lost with

cells orienting randomly on substrates with groove spacings smaller than 50 nm.

Data accessibility. This manuscript does not report primary experimental data. All relevant simulation parameters have been detailed in the main text and electronic supplementary material.

Author contributions. V.S.D. conceived the study. V.S.D. and R.M.Mc.M. devised the mathematical models. A.V. implemented the mathematical models and produced the numerical results. V.S.D. wrote the paper. R.M.Mc.M. and A.V. contributed to the revision of the paper.

Funding statement. A.V. and V.S.D. acknowledge the Royal Society for supporting A.V. through a Newton International Fellowship.

Competing interests. We have no competing interests.

Endnotes

[1]Note that the transformation of integrins from the high- to the low-affinity state (resulting in a negative ξ_H) does not contribute towards Rho activation.

[2]We make the contribution of the additional signal generation explicit in the electronic supplementary material.

References

1. Engler AJ, Sen S, Sweeney HL, Discher DE. 2006 Matrix elasticity directs stem cell lineage specification. *Cell* **126**, 677–689. (doi:10.1016/j.cell.2006.06.044)
2. Nelson CM, Jean RP, Tan JL, Liu WF, Sniadecki NJ, Spector AA, Chen CS. 2005 Emergent patterns of growth controlled by multicellular form and mechanics. *Proc. Natl Acad. Sci. USA* **102**, 11 594–11 599. (doi:10.1073/pnas.0502575102)
3. McBeath R, Pirone DM, Nelson CM, Bhadriraju K, Chen CS. 2004 Cell shape, cytoskeletal tension, and RhoA regulate stem cell lineage commitment. *Dev. Cell* **6**, 483–495. (doi:10.1016/S1534-5807(04)00075-9)
4. McMurray RJ *et al*. 2011 Nanoscale surfaces for the long-term maintenance of mesenchymal stem cell phenotype and multipotency. *Nat. Mater.* **10**, 637–644. (doi:10.1038/nmat3058)
5. Weiner S, Wagner HD. 1998 The material bone: structure mechanical function relations. *Annu. Rev. Mater. Sci.* **28**, 271–298. (doi:10.1146/annurev.matsci.28.1.271)
6. Hansen JC, Lim JY, Xu LC, Siedlecki CA, Mauger DT, Donahue HJ. 2007 Effect of surface nanoscale topography on elastic modulus of individual osteoblastic cells as determined by atomic force microscopy. *J. Biomech.* **40**, 2865–2871. (doi:10.1016/j.jbiomech.2007.03.018)
7. Lim JY, Hansen JC, Siedlecki CA, Hengstebeck RW, Cheng J, Winograd N, Donahue HJ. 2005 Osteoblast adhesion on poly(L-lactic acid)/polystyrene demixed thin film blends: effect of nanotopography, surface chemistry, and wettability. *Biomacromolecules* **6**, 3319–3327. (doi:10.1021/bm0503423)
8. Dalby MJ, McCloy D, Robertson M, Wilkinson CDW, Oreffo ROC. 2006 Osteoprogenitor response to defined topographies with nanoscale depths. *Biomaterials* **27**, 1306–1315. (doi:10.1016/j.biomaterials.2005.08.028)
9. Guido S, Tranquillo RT. 1993 A methodology for the systematic and quantitative study of cell contact guidance in oriented collagen gels—correlation of fibroblast orientation and gel birefringence. *J. Cell Sci.* **105**, 317–331.
10. Tranquillo RT. 1999 Self-organization of tissue-equivalents: the nature and role of contact guidance. *Cell Behav.* **65**, 27–42.
11. Foolen J, Deshpande VS, Kanters FMW, Baaijens FPT. 2012 The influence of matrix integrity on stress-fiber remodeling in 3D. *Biomaterials* **33**, 7508–7518. (doi:10.1016/j.biomaterials.2012.06.103)
12. Eastwood M, Mudera VC, McGrouther DA, Brown RA. 1998 Effect of precise mechanical loading on fibroblast populated collagen lattices: morphological changes. *Cell Motil. Cytoskeleton* **40**, 13–21. (doi:10.1002/(SICI)1097-0169(1998)40:1<13::AID-CM2>3.0.CO;2-G)
13. Henshaw DR, Attia E, Bhargava M, Hannafin LA. 2006 Canine ACL fibroblast integrin expression and cell alignment in response to cyclic tensile strain in three-dimensional collagen gels. *J. Orthop. Res.* **24**, 481–490. (doi:10.1002/jor.20050)
14. Rubbens MP, Driessen-Mol A, Boerboom RA, Koppert MMJ, van Assen HC, Romeny BMT, Baaijens FPT, Bouten CVC. 2009 Quantification of the temporal evolution of collagen orientation in mechanically conditioned engineered cardiovascular tissues. *Ann. Biomed. Eng.* **37**, 1263–1272. (doi:10.1007/s10439-009-9698-x)
15. Tan JL, Tien J, Pirone DM, Gray DS, Bhadriraju K, Chen CS. 2003 Cells lying on a bed of microneedles: an approach to isolate mechanical force. *Proc. Natl Acad. Sci. USA* **100**, 1484–1489. (doi:10.1073/pnas.0235407100)
16. Lamers E, Walboomers XF, Domanski M, te Riet J, van Delft FCMJM, Luttge R, Winnubst LAJA, Gardeniers HJGE, Jansen JA, 2010 The influence of nanoscale grooved substrates on osteoblast behavior and extracellular matrix deposition. *Biomaterials* **31**, 3307–3316. (doi:10.1016/j.biomaterials.2010.01.034)
17. Deshpande VS, McMeeking RM, Evans AG. 2006 A bio-chemo-mechanical model for cell contractility. *Proc. Natl Acad. Sci. USA* **103**, 14 015–14 020. (doi:10.1073/pnas.0605837103)
18. Obbink-Huizer C, Oomens CWJ, Loerakker S, Foolen J, Bouten CVC, Baaijens FPT. 2014 Computational model predicts cell orientation in response to a range of mechanical stimuli. *Biomech. Model. Mechanobiol.* **13**, 227–236. (doi:10.1007/s10237-013-0501-4)
19. Vernerey FJ, Farsad M. 2011 A constrained mixture approach to mechano-sensing and force generation in contractile cells. *J. Mech. Behav. Biomed. Mater.* **4**, 1683–1699. (doi:10.1016/j.jmbbm.2011.05.022)
20. Stalhand J, Klarbring A, Holzapfel GA. 2011 A mechanochemical 3D continuum model for smooth muscle contraction under finite strains. *J. Theor. Biol.* **268**, 120–130. (doi:10.1016/j.jtbi.2010.10.008)
21. McGarry JP, Fu J, Yang MT, Chen CS, McMeeking RM, Evans AG, Deshpande VS. 2009 Simulation of the contractile response of cells on an array of micro-posts. *Phil. Trans. R. Soc. A* **367**, 3477–3497. (doi:10.1098/rsta.2009.0097)
22. Wei ZS, Deshpande VS, McMeeking RM, Evans AG. 2008 Analysis and interpretation of stress fiber organization in cells subject to cyclic stretch. *J. Biomech. Eng.* **130**, 031009. (doi:10.1115/1.2907745)
23. Ronan W, Deshpande VS, McMeeking RM, McGarry JP. 2012 Numerical investigation of the active role of the actin cytoskeleton in the compression resistance of cells. *J. Mech. Behav. Biomed. Mater.* **14**, 143–157. (doi:10.1016/j.jmbbm.2012.05.016)
24. Deshpande VS, Mrksich M, McMeeking RM, Evans AG. 2008 A bio-mechanical model for coupling cell contractility with focal adhesion formation. *J. Mech. Phys. Solids* **56**, 1484–1510. (doi:10.1016/j.jmps.2007.08.006)
25. Pathak A, Deshpande VS, McMeeking RM, Evans AG. 2008 The simulation of stress fibre and focal adhesion development in cells on patterned substrates. *J. R. Soc. Interface* **5**, 507–524. (doi:10.1098/rsif.2007.1182)
26. Pathak A, McMeeking RM, Evans AG, Deshpande VS. 2011 An analysis of the cooperative mechano-sensitive feedback between intracellular signaling, focal adhesion development, and stress fiber contractility. *J. Appl. Mech.* **78**, 041001. (doi:10.1115/1.4003705)
27. Hill AV. 1938 The heat of shortening and the dynamic constants of muscle. *Proc. R. Soc. Lond. B* **126**, 136–195. (doi:10.1098/rspb.1938.0050)
28. Lennard-Jones JE. 1931 Cohesion. *Proc. Phys. Soc.* **43**, 461–482. (doi:10.1088/0959-5309/43/5/301)
29. Oakes PW, Gardel ML. 2014 Stressing the limits of focal adhesion mechanosensitivity. *Curr. Opin. Cell Biol.* **30**, 68–73. (doi:10.1016/j.ceb.2014.06.003)

30. Théry M, Pépin A, Dressaire E, Chen Y, Bornens M. 2006 Cell distribution of stress fibres in response to the geometry of the adhesive environment. *Cell Motil. Cytoskeleton* **63**, 341–355. (doi:10.1002/cm.20126)
31. Tanner K, Boudreau A, Bissell MJ, Kumar S. 2010 Dissecting regional variations in stress fiber mechanics in living cells with laser nanosurgery. *Biophys. J.* **99**, 2775–2783. (doi:10.1016/j.bpj.2010.08.071)
32. Otsuji M, Ishihara S, Co C, Kaibuchi K, Mochizuki A, Kuroda S. 2007 A mass conserved reaction–diffusion system captures properties of cell polarity. *PLoS Comput. Biol.* **3**, 1040–1054. (doi:10.1371/journal.pcbi.0030108)
33. Lauffenburger DA, Linderman JJ. 1996 *Receptors: models for binding, trafficking, and signalling*. Oxford, UK: Oxford University Press.
34. Leckband D, Israelachvili J. 2001 Intermolecular forces in biology. *Q. Rev. Biophys.* **34**, 105–267. (doi:10.1017/S0033583501003687)
35. McCleverty CJ, Liddington RC. 2003 Engineered allosteric mutants of the integrin aMb2 I domain: structural and functional studies. *Biochem. J.* **372**, 121–127. (doi:10.1042/BJ20021273)
36. Merkel R, Nassoy P, Leung A, Ritchie K, Evans E. 1999 Energy landscapes of receptor–ligand bonds explored with dynamic force spectroscopy. *Nature* **397**, 50–53. (doi:10.1038/16219)
37. Kaunas R, Nguyen P, Usami S, Chien S. 2005 Cooperative effects of Rho and mechanical stretch on stress fiber organization. *Proc. Natl Acad. Sci. USA* **102**, 15 895–15 900. (doi:10.1073/pnas.0506041102)